JOURNAL OF MATERIALS SCIENCE 33 (1998) 3391–3400

Mechanical and photoelastic properties of oriented poly-4-methyl-1-pentene investigated by Brillouin spectroscopy

S. H. ANDERS, R. EBERLE, M. PIETRALLA
Abteilung für Experimentelle Physik, Universität Ulm, Albert-Einstein-Allee II, 89069 Ulm, Germany
E-mail: martin.pietralla@physik.uni-ulm.de

The elastic constants C_{11}, C_{13}, C_{33} and C_{44} of oriented poly-4-methyl-1-pentane (P4M1P) films were measured with Brillouin scattering. The photoelastic constants p_{11}, p_{13}, p_{31} and p_{33} were measured by evaluating the integral intensities of the phonon lines. The correlation of the photoelastic constants p_{13} and p_{31} with the degree of stretching was determined by evaluating the relative integral intensities of the Brillouin lines with the phonon propagation vector into and perpendicular to the stress direction. The other photoelastic constants were measured by comparing the angle-dependent relative integral intensities of the transverse and longitudinal Brillouin lines. The elastic constants, as well as birefringence, were surprisingly found to be unaffected by further stretching of the sample above the necking region. The density was constant for all degrees of stretching. The photoelastic constants p_{11} and p_{33} showed significant variation during deformation. The results have been compared with former measurements of polypropylene (PP) by Cavanaugh and Wang. Because the elastic constants are unchanged during deformation, the modulation of the intensities is due to the variation of the photoelastic constants for this material. © *1998 Kluwer Academic Publishers*

1. Introduction

Brillouin scattering has been used for more than two decades for studying the elastic and relaxational properties of polymers. The directional properties of hypersound propagation in oriented polymers have been explored for different amorphous and semicrystalline polymers such as polycarbonate (PC) [1, 2], polymethylmethacrylate (PMMA) [3], polyethyleneterephthalate (PET) [4], polyvinylfluoride (PVF) [5], polypropylene (PP) [6, 7] and polyethylene (PE) [8]. Relaxational phenomena, which require either the evaluation of the full-width at half-maximum (FWHM) or a special combination of scattering geometries, has been studied for example, for PPG [9], polyisoprene [10] and polysiloxane [11–13]. The integral intensity of the phonon lines is related to the photoelastic tensor, which can give additional information regarding the processes causing the orientation inside a sample. The photoelastic tensor describes the effect of small elastic deformations on the dielectric tensor and therefore the refractive index. Although the integral intensity is easily accessible if a suitable function is used for the description of the spectra, it has seldomly been evaluated. To our knowledge, only Wang and co-workers have investigated the dependence of the photoelastic tensor components on the degree of stretching for polycarbonate [1] and polypropylene [6]. For measurements of the photoelastic tensor, often special polarization geometries are applied, which are useful for the detection of, for example, weak transverse phonons beneath strong longitudinal lines. Longitudinal Brillouin lines can be observed with a VV scattering geometry (incident and detected light vertically polarized), while transverse Brillouin lines can be more easily detected using a VH geometry (detected light horizontally polarized). In this work we show that is also possible to measure the photoelastic tensor with the simpler VA geometry (all polarization directions detected), which also has the advantage of a larger scattered intensity and is therefore favourable due to shorter accumulation time.

2. Experimental procedure

2.1. Sample preparation

Poly-4-methyl-1-penten (P4M1P) was donated by Mitsui (Japan) as a film (RT18) with 200 μm initial thickness. Standard formed pieces were cut out using a press. The films were drawn with a Zwick 1440 tensile testing machine at 100 °C, which is above the glass temperature, T_G, but below the melting temperature of the crystalline parts (cf. Table I). Films with draw ratios of $\lambda = 1.0, 4.3, 5.4, 5.9, 6.5$ were prepared. The slowest possible stretching speed (0.5% min^{-1}) was used.

0022–2461

TABLE I Sample data of P4M1P

Melting temperature, T_M [16]	235 °C
Glass temperature, T_G [16]	30 °C
Density [16]	0.834 g cm^{-3}
Molecular weight, M_W	406690 g mol^{-1}
M_W/M_N	1.8

Additionally, an extruded rod with a diameter of approximately 1.5 mm was prepared by Kanamoto and co-workers [14, 15] through extruding with a hydrostatic pressure of 1200 atm, a temperature of 200 °C and a velocity of 1 mm min^{-1}. The degree of stretching computed by comparing the diameter of the rod before and after extruding is approximately 60. The density of the samples was measured by density gradient method. It was identical for all samples. The value of 0.834 g cm^{-3} agrees with the value supplied by the manufacturer [16].

2.2. Birefringence measurements

The birefringence of the film samples was measured using a polarization microscope (Leitz) with tilt compensators (Ehringhaus, type 697K and 1054K).

2.3. WAXS measurements

Wide-angle X-ray spectroscopy (WAXS) diffraction patterns were measured with a self-built flat-plate camera and a Philips PW1120/00 X-ray-generator (tube PW2213/40, Cu-K_α line).

2.4. Spectra recording

The spectrometer consists of a piezoelectrically scanned Fabry-Perot-Interferometer from Burleigh Instruments. Spectra were accumulated in a five-pass arrangement. The free spectral range (FSR) of the interferometer was 10.93 GHz. The light source was a frequency doubled Nd–YAG laser (DPSS-532 with 450 mW, Coherent, USA) with vertical polarization. Because of the high Rayleigh intensity, the incident light was modulated by a Pockels cell. A 90A–VA scattering geometry (90° antireflex geometry, incoming light vertically polarized, all polarization directions detected) [17] was used (Fig. 1). All experiments were performed at room temperature.

The sound velocity contours of the anisotropic samples were determined with a computer-controlled goniometer possessing an angular setting accuracy of 0.006 °. The angle, α, associated with the sound velocity is the angle included by the direction of the stress and the phonon wave vector, q. Thus when $\alpha = 0°$, q is parallel to the direction of stress (= z-axis, "3"). If $\alpha = 90°$, q is perpendicular to that direction (= x-axis, "1"). The y-axis "2" is perpendicular to the x- and z-axes (Fig. 1). Vector components are denoted with letters while for tensor components numbers are employed.

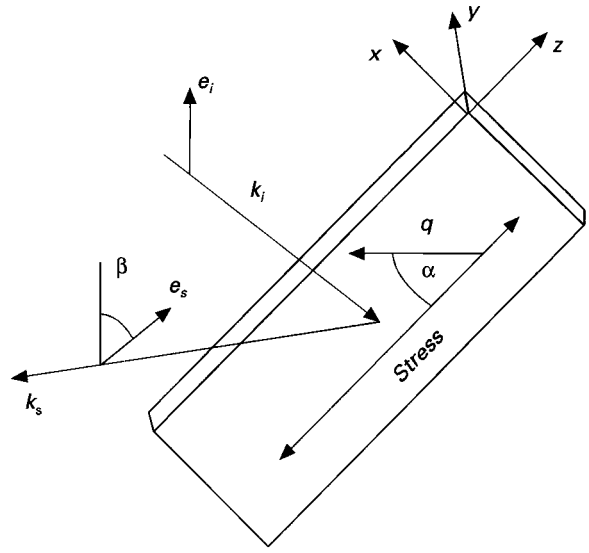

Figure 1 The scattering geometry used in this work. k_i and k_s are perpendicular to each other. The stretched film bisects this angle. α is the angle of the scattering vector against the stretching direction.

2.5. Data evaluation

The spectra were fitted to a set of Pearson type VII [18] functions attaining the full-width at half-maximum (FWHM), height and frequency shift of the Brillouin lines. The integral intensity of a line is computed by a numerical integration [19] of a Pearson type VII shaped line with the parameters gained from the fitting procedure. From the frequency shift, ω, and scattering vector, q, the sound velocity, v, is computed as

$$v = \frac{\omega}{q} \tag{1a}$$

$$q = 2|K_i| \sin\frac{\theta}{2} \tag{1b}$$

(for details see [17]).

3. Theory: elastic and photoelastic properties in samples exhibiting hexagonal symmetry

3.1. Sound waves in anisotropic solids

The field equations for sound waves in the continuum can be derived from the laws of conservation of mass, momentum, energy and angular momentum (cf. eg. [8, 20, 21]). The conservation of mass leads to the equation of continuity

$$\frac{d\rho}{dt} + \rho div\,\xi = 0 \tag{2}$$

From the conservation of momentum the Cauchy equation of motion is deduced, which is

$$Div^2\sigma - \rho \cdot \frac{\partial \xi}{\partial t} = 0 \tag{3}$$

in linear approximation for non-polar materials in the absence of external forces and damping. The density of

mass $\rho = \rho(r, t)$ depends on time t and location r. ξ (r, t) is the velocity of the particles calculated by partially differentiating the displacement field $s(r, t)$ with respect to time. $^2\sigma(r, t)$ is the stress tensor fully describing the state of stress of the system. *div* is the vector divergence and *Div* the tensor divergence. For small deformations the stress depends linearly on the strain, ε, as formulated by Hooke's law where ^4C is the tensor of the elastic constants

$$^2\sigma = {}^4C \cdot {}^2\varepsilon \tag{4}$$

$^2\varepsilon$ is the symmetric part of displacement tensor ^2s which is defined as

$$s_{i,k} = \frac{\partial s_i}{\partial x_k} \tag{5}$$

$$\varepsilon_{ik} = \tfrac{1}{2}(s_{l,k} + s_{k,l}) \tag{6}$$

The equation of motion for a solid derived from Equations 2 and 3 is

$$\rho \ddot{s}_i = C_{ijkl} \frac{\partial^2 s_l}{\partial x_j \partial x_k} \tag{7}$$

The summation convention is applied. One solution of this equation has the form of plane sinusoidal waves

$$s_\sigma(r, t) = e_\sigma s_\sigma e^{l(qr - \omega_{q\sigma})} \tag{8}$$

where σ is the index (longitudinal or transverse), e_σ the polarization vector and $\hat{s}_\sigma$ the amplitude of a sound mode travelling into the direction e_n with the wave vector $q = qe_n$. The value of the sound wave vector is defined by the wavelength, Λ, or the phase velocity of the mode $v_{q\sigma}$ and its frequency $\omega_{q\sigma}$

$$q = qe_n = \frac{\omega_{q\sigma}}{v_{q\sigma}} \cdot e_n = \frac{2 \cdot \pi}{\Lambda} \cdot e_n \tag{9}$$

For plane sinusoidal waves the phase velocities and polarizations of sound modes can be determined by solving the equation

$$\{e_n \cdot {}^4C \cdot e_n - \rho v_{q\sigma}^2(e_n) \cdot {}^2\delta\} \cdot e_\sigma = 0 \tag{10}$$

Using the Christoffel tensor, Γ, the according eigenvalue equation reads as

$$|{}^2\Gamma(e_n) - \rho \cdot v_{q\sigma}^2(e_n) \cdot {}^2\delta| = 0 \tag{11}$$

The eigenvalues are the three sound velocities that are observable in a solid.

3.2. Solution of the sound wave equation for the case of hexagonal symmetry

A uniaxial deformation will change the symmetry of a sample from isotropic to hexagonal. The symmetry is uniaxial ∞-fold. The elastic tensor, however, is the same as that of a hexagonal system. Orthorhombic symmetries can occur due to transverse stresses in this films [4]. In cases of hexagonal symmetry, the elastic tensor has the form (using the known Voigt notation)

$$C_{ijkl} = \begin{bmatrix} C_{11} & C_{12} & C_{13} & 0 & 0 & 0 \\ C_{12} & C_{11} & C_{13} & 0 & 0 & 0 \\ C_{13} & C_{13} & C_{33} & 0 & 0 & 0 \\ 0 & 0 & 0 & C_{44} & 0 & 0 \\ 0 & 0 & 0 & 0 & C_{44} & 0 \\ 0 & 0 & 0 & 0 & 0 & C_{66} \end{bmatrix} \tag{12}$$

The subsequently required photoelastic tensor is similar to the elastic one

$$p_{ijkl} = \begin{bmatrix} p_{11} & p_{12} & p_{13} & 0 & 0 & 0 \\ p_{12} & p_{11} & p_{13} & 0 & 0 & 0 \\ p_{13} & p_{13} & p_{33} & 0 & 0 & 0 \\ 0 & 0 & 0 & p_{44} & 0 & 0 \\ 0 & 0 & 0 & 0 & p_{44} & 0 \\ 0 & 0 & 0 & 0 & 0 & p_{66} \end{bmatrix} \tag{13}$$

The tensor components C_{66} and p_{66} are given by

$$\begin{aligned} C_{66} &= \tfrac{1}{2}(C_{11} - C_{12}) \\ p_{66} &= \tfrac{1}{2}(p_{11} - p_{12}) \end{aligned} \tag{14}$$

From the tensor components, the sound velocities are computed as follows.

$$\begin{aligned} 2\rho V_\pm^2 &= A \pm (B^2 - 4[C \cdot D - E])^{1/2} \\ A &= B = C_{11}\sin^2\alpha + C_{33}\cos^2\alpha + C_{44} \\ C &= C_{11}\sin^2\alpha + C_{44}\cos^2\alpha \\ D &= C_{33}\cos^2\alpha + C_{44}\sin^2\alpha \\ E &= \sin^2\alpha\cos^2\alpha(C_{13} + C_{44})^2 \end{aligned} \tag{15}$$

V_+ refers to the quasi-longitudinal and V_- to the quasi-transverse wave. The third solution is the pure transverse mode

$$V_{pt} = \left(\frac{C_{66}\sin^2\alpha + C_{44}\cos^2\alpha}{\rho}\right)^{1/2} \tag{16}$$

3.3. Photoelastic properties of anisotropic solids

The intensity of the Brillouin scattered light is the square of the amplitude of the scattered electromagnetic field, E_s. It depends on the variation of the dielectric tensor due to the movement of the particles caused by the sound wave. In the far-field limit

one gets [22]

$$E_s(R,t) = A(R)\int_V \boldsymbol{e}_s \cdot [\boldsymbol{k}_s \times \boldsymbol{k}_s \times [(\delta^2\boldsymbol{\varepsilon}(\boldsymbol{r},t)\cdot \boldsymbol{e}_l]] \cdot e^{i\boldsymbol{q}\boldsymbol{r}} d^3\boldsymbol{r}$$

$$= A(R)k_s^2 \cdot e^{I(k_s R-\omega t)} \cdot \frac{1}{2\pi} \cdot \delta\varepsilon_{ls}(q,t) \qquad (17a)$$

$$A(R) = \frac{E_0}{4\pi\varepsilon_0 R} \qquad (17b)$$

where E_0 is the amplitude of the electro-magnetic field of the incident light, and ε_0 is the dielectric constant in a vacuum.

The intensity of the scattered light at a distance R and time t into the direction q therefore becomes

$$I_{is}(\boldsymbol{q},\omega_s,R = A^2(R)K_s^4 \cdot \frac{1}{2\pi} \cdot \langle|\delta\varepsilon_{ls}(\boldsymbol{q},\omega)|^2\rangle \qquad (18)$$

The displacement gradient $\delta s_m/\delta x_n$ (usually denominated ε_{mn}, cf. Equation 4) couples via the Pockelstensor to fluctuations of the inverse dielectric tensor [23, 24]

$$(\delta\varepsilon)_{kl}^{-1} = p_{klmn}\frac{\partial s_m}{\partial x_n} \qquad (19)$$

The fluctuations of the dielectric tensor are computed from the fluctuations of the inverse dielectric tensor with the help of the principal indices of refraction n_k by [6]

$$\delta\varepsilon_{is} = -\varepsilon_{ik}^0 \cdot \varepsilon_{sl}^0 \cdot (\delta\varepsilon^{-1})_{kl}$$

$$\varepsilon_{ik}^0 = n_k^2 \cdot e_{ik} \qquad (20)$$

Therefore, the scattered intensity computed by Equations 17–20 is

$$I_{is}^s = A^2(R)k_s^4 \cdot \left\langle \left| \sum_{klmn} n_k^2 n_l^2 e_{i\cdot k} e_{s\cdot l} p_{klmn} s_m(\boldsymbol{q}) q_n \right|^2 \right\rangle \qquad (21)$$

The expression can be simplified by introducing the Brillouintensor

$${}^2\boldsymbol{T}_{q\sigma} = {}^2\varepsilon \cdot (\boldsymbol{e}_n \cdot {}^4\boldsymbol{p} \cdot \boldsymbol{e}_6) \cdot {}^2\varepsilon \qquad (22)$$

$$I_{is}^s = A^2(R)k_s^4 \cdot \sum_{\sigma=1}^{3} V^2 q^2 \boldsymbol{e}_s \cdot {}^2T_{q\sigma} \cdot \boldsymbol{e}^2 \langle|s(\boldsymbol{q})|^2\rangle \qquad (23)$$

This equation relates the scattered intensity to the displacement of the particles by the sound wave through Equation 19 (cf. Fig. 2). For intensity measurements the 90A geometry is advantageous because the refractive index is not involved in the computation of the sound velocity, thus leading to a better overall accuracy. In this setup the components of the scattering vector $\boldsymbol{q}$ are

$$q_x = -\sin\alpha \qquad (24a)$$

$$q_y = 0 \qquad (24b)$$

$$q_z = \cos\alpha \qquad (24c)$$

The relative amplitude of the sound waves can be computed from Equation 11 by inserting the wave vector q.

$$-(C_{11}\sin^2\alpha + C_{44}\cos^2\alpha - \rho V_{\pm}^2)s_x$$

$$= [(C_{13} + C_{44})\sin\alpha\cos\alpha]s_z \qquad (25)$$

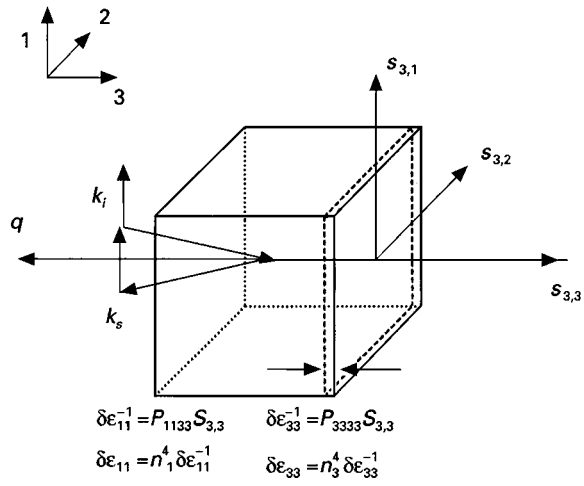

Figure 2 Scattering of vertically polarized light by a longitudinal sound wave travelling into the draw direction. In the case of hexagonal symmetry, the Pockets coefficients p_{ij33}, with $i \neq j$, are zero. Therefore, the resulting dielectric tensor is diagonal. In geometries with the incoming light being vertically polarized, only the first tensor component contributes to scattering. Because the sound propagates into direction 3 and the light is polarized into direction 1 only p_{1133} influences the scattered intensity. If the sample is turned to an angle of $\alpha = 90°$, only p_{3311} is required as the sound wave vector points into direction 1 and the light polarization vector points into direction 3.

For further computations, the normalized amplitudes are used

$$S_x^2 + S_y^2 + S_z^2 = 1 \qquad S_y = 0 \qquad (26)$$

Because the pure transverse mode was not observed in our experiments, in the following section, only scattered intensities from quasi-longitudinal or quasi-transverse waves are treated. The results for the transverse mode are similar, but the form differs slightly.

3.4. Scattering intensities in the VV geometry

In this geometry, the incident and the detected light are vertically polarized. The projections of the polarizations onto the direction of stress $c_{i\cdot x} = e_i \cdot e_x$ *are*

$$e_{l\cdot x} = e_{s\cdot x} = \cos\alpha$$

$$e_{i\cdot y} = e_{s\cdot y} = 0 \qquad (27)$$

$$e_{i,z} = e_{s,z} = \sin\alpha$$

The intensity scattered by a sound mode is

$$I_{is}^S = A^2(R)K_S^4\langle|n_x^4\cos^2\alpha(-p_{11}\sin\alpha s_x + p_{13}\cos\alpha s_z)$$

$$+ 2n_x^2 n_z^2\cos\alpha\sin\alpha(p_{44}\cos\alpha s_x - p_{44}\sin\alpha s_z)$$

$$+ n_z^4\sin^2\alpha(-p_{31}\sin\alpha s_x + p_{33}\cos\alpha s_z)|^2\rangle \qquad (28)$$

For each sound mode, the amplitudes must be seperately determined, i.e. the displacement vectors are different for different sound modes.

3.5. Scattering intensities in the VH geometry

In this geometry, the incident light is vertically polarized and the analysed light is horizontally polarized.

The projections of the polarizations on to the direction of stress are

$$e_{i\cdot 1} = \cos\alpha \qquad e_{s\cdot 1} = -\sin\alpha\cos\frac{\theta}{2} \tag{29a}$$

$$e_{i\cdot 2} = 0 \qquad e_{s\cdot 2} = -\sin\frac{\theta}{2} \tag{29b}$$

$$e_{i\cdot 3} = \sin\alpha \qquad e_{s\cdot 3} = \cos\alpha\cos\frac{\theta}{2} \tag{29c}$$

and the resulting intensity is

$$\begin{aligned} I_{is}^{S} = A^2(R)k_S^4\langle|&n_x^4\cos\alpha\sin\alpha\cos\frac{\theta}{2} \\ &\times(p_{11}\sin\alpha s_x - p_{13}\cos\alpha s_z) \\ &+ n_x^2 n_z^2\left(\sin^2\alpha\cos\frac{\theta}{2} - \cos^2\alpha\cos\frac{\theta}{2}\right) \\ &\times(p_{44}\sin\alpha s_z - p_{44}\cos\alpha s_x) \\ &+ n_z^4\sin\alpha\cos\alpha\cos\frac{\theta}{2} \\ &\times(-p_{31}\sin\alpha s_x + p_{33}\cos\alpha s_z)|^2\rangle \end{aligned} \tag{30}$$

Almost all measurements of the photoelastic constants have been performed utilizing one of the above polarization geometries. Using all of the scattered light and not only the polarized or depolarized components would result in a significantly lower accumulation time of the spectra. We will now compute the scattered intensities in the VA geometry.

3.6. Scattering intensities in the VA geometry

In this geometry, the incident light is vertically polarized. All of the scattered light is detected. The projections of the polarizations on to the direction of stress are

$$e_{i\cdot 1} = \cos\alpha \quad e_{s\cdot 1} = \cos\alpha\cos\beta - \cos\alpha\sin\alpha\sin\beta\cos\frac{\theta}{2} \tag{31a}$$

$$e_{i\cdot 2} = 0 \quad e_{s\cdot 2} = -\sin\frac{\theta}{2}\sin\beta \tag{31b}$$

$$e_{i,3} = \sin\alpha \quad e_{s,3} = \sin\alpha\cos\beta + \cos\alpha\sin\beta\cos\frac{\theta}{2} \tag{31c}$$

In this case, the scattering intensity has to be computed for an arbitrary angle, β.

We obtain

$$\begin{aligned} I_{is}^{s}(\beta) = A^2(R)k_s^4 &\cdot\left\langle\left|n_x^4\left(\cos^2\alpha\cos\beta - \cos\alpha\sin\alpha\sin\beta\cos\frac{\theta}{2}\right)B\right.\right. \\ &+ n_x^2 n_z^2\left(\cos\alpha\sin\alpha\cos\beta + \cos^2\alpha\sin\beta\cos\frac{\theta}{2}\right)C \\ &+ n_x^2 n_z^2\left(\cos\alpha\sin\alpha\cos\beta - \sin^2\alpha\sin\beta\cos\frac{\theta}{2}\right)C \\ &\left.\left.+ n_z^4\left(\sin^2\alpha\cos\beta + \cos\alpha\sin\beta\cos\frac{\theta}{2}\right)D\right|^2\right\rangle \end{aligned} \tag{32a}$$

$$B = -p_{11}\sin\alpha s_x + p_{13}\cos\alpha s_z \tag{32b}$$

$$C = -p_{44}\sin\alpha s_z + p_{44}\cos\alpha s_x \tag{32c}$$

$$D = -p_{31}\sin\alpha s_x + p_{33}\cos\alpha s_z \tag{32d}$$

The total intensity is determined by computing the integral over all angles β (p_{44} has been set to zero because the pure transverse mode is not observable)

$$\begin{aligned} I_{is}^{s} &= \int_0^{2\pi} I_{is}^{s}(\beta)\,d\beta \\ &= A^2(R)k_s^4\cdot\Big((B^2 + D^2)\cdot\sin^2\alpha\cdot\cos^2\alpha\cdot\cos^2\frac{\theta}{2} \\ &\quad + 2BD\sin^2\alpha\cdot\cos^2\alpha\cdot\sin^2\frac{\theta}{2} + B^2\cdot\cos^4\alpha \\ &\quad + D^2\cdot\sin^4\alpha\Big) \end{aligned} \tag{33}$$

It is evident from Equation 32a that for $\alpha = 0°$ only p_{13} settles the intensity, while for $\alpha = 90°$ only p_{31} is required. This is also valid for the other polarization geometries (Fig. 2).

3.7. Data handling

The elastic constants were calculated by a simultaneous non-linear fit [19] of the quasi-transverse and quasi-longitudinal sound velocity to Equation 15. For the computation of the photoelastic constants, the relative scattered intensity (i.e. the intensity of the transverse Brillouin line divided by the intensity of the longitudinal line) as well as the elastic constants and the sound velocities in the selected direction, are needed. We used the calculated sound velocity instead of the measured one for a better overall accuracy. As the photoelastic constants cannot be determined absolutely with this method [6], only relative values can be given. p_{13} and p_{31} were determined by taking the root of the intensities of the longitudinal mode parallel and perpendicular to the drawing direction. p_{11} and p_{33} were subsequently determined by a non-linear fit to the angular scan of intensities, in which p_{13} and p_{31} were fixed. As the birefringence is very small it is neglected for the evaluation of the photoelastic coefficients.

4. Results and discussion

Two sound modes have been observed, the quasi-longitudinal and the quasi-transverse. Similar to many other polymers, no pure transverse mode was detected. Therefore, C_{66} could not be determined. Fig. 3 shows sample spectra of the P4M1P-films at $\lambda = 4.29$ and $\lambda = 6.51$ observed at $\alpha = 30°$. The relative scattered intensities of the quasi-longitudinal and quasi-transverse lines increase with deformation, while the positions of the lines do not change that much. For

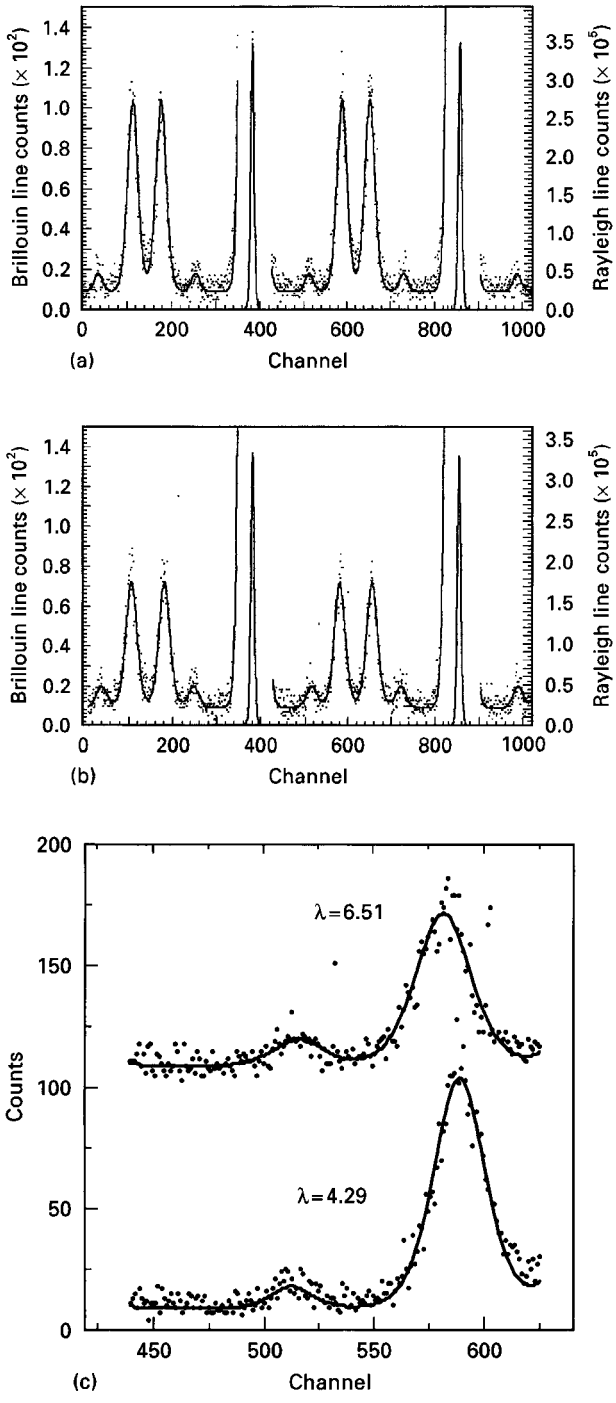

Figure 3 Brillouin spectra of P4M1P films stretched to a draw ratio of (a) 4.29 and (b) 6.52 at $\alpha = 40°$. Note that the Rayleigh intensity is almost identical in (a) and (b). (c) The Brillouin band of both spectra, showing that the intensity of the longitudinally scattered light is decreasing while the intensity of the transversely scattered light is apparently constant.

comparison, in Fig. 4, the elastic constants C_{11}, C_{13}, C_{33} and C_{44} of PE, PP and P4M1P (Table II) are plotted versus the deformation. The variation of these constants with the draw ratio is very small in the films ($\lambda = 4.5$–6.5); even in the extruded rod the values for C_{11} and C_{33} resemble the values measured in the films. The striking contrast of P4M1P compared to PE and PP is the small optical and mechanical anisotropy (Figs 5 and 6) despite a high molecular orientation as revealed by WAXS and infrared-dichroism [25]. Birefringence averages polarizabilities. Thus the side groups give a noticeable contribution to the perpendicularly

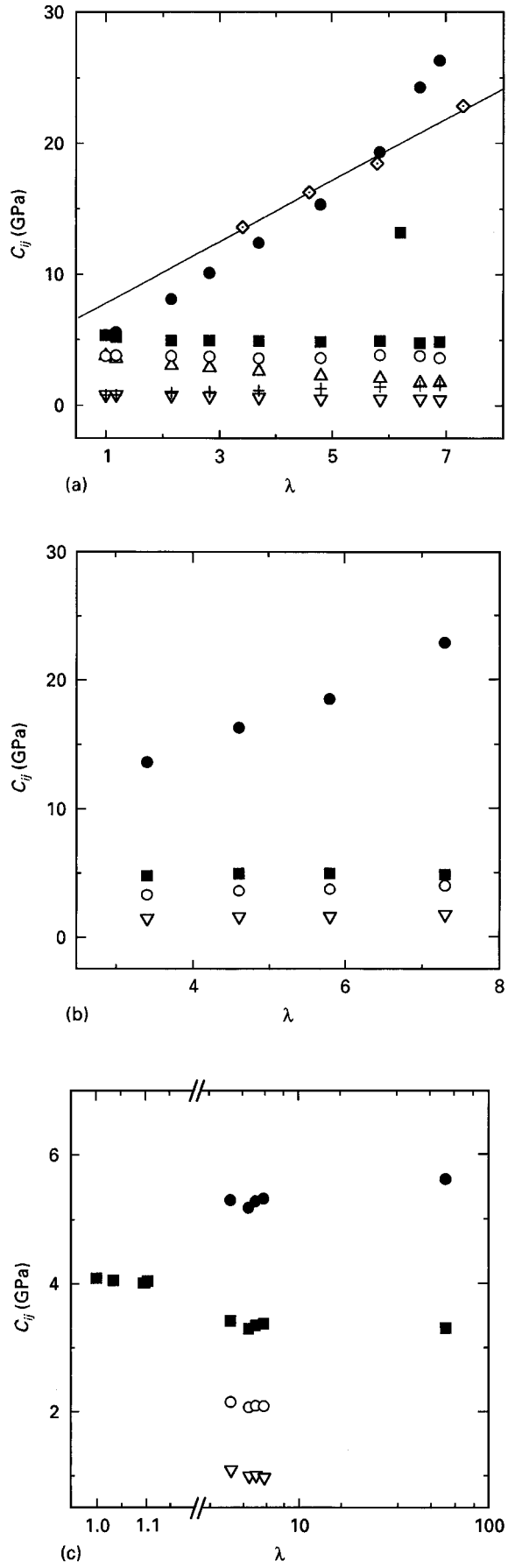

Figure 4 Elastic constants of (a) polyethylene, (b) polypropylene and (c) P4M1P. The slope of C_{33} decreases with bigger side groups. For P4M1P it is almost zero. (■) C_{11}, (△) C_{12}, (○) C_{13}, (●) C_{33}, (▽) C_{44}, (+) C_{66}, (♦) C_{33} pp.

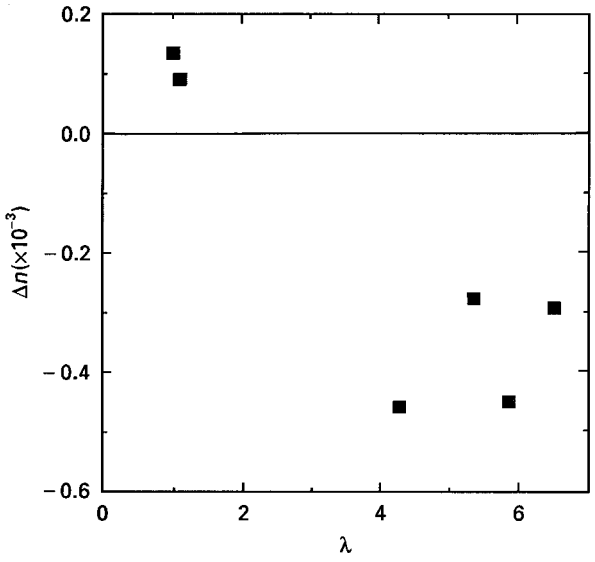

Figure 5 Birefringence in oriented P4M1P. The values are very small compared to, for example, PE [8], and stay almost constant for larger draw ratios.

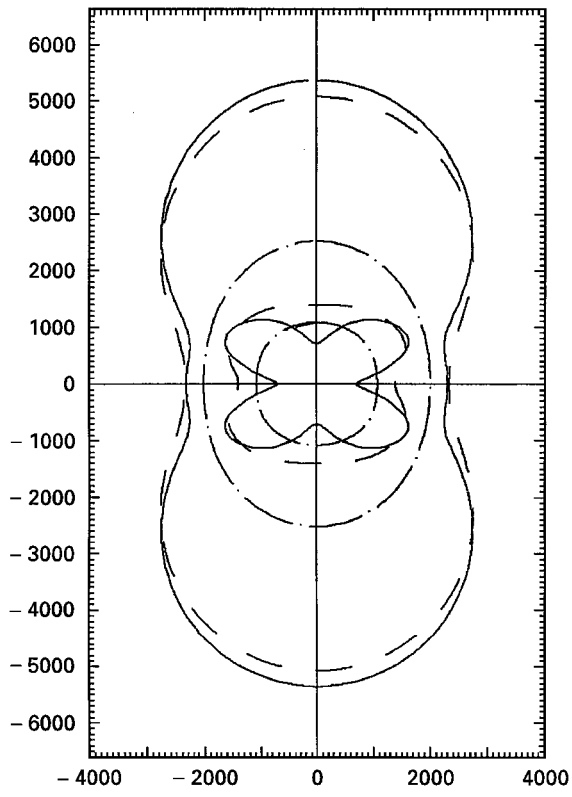

Figure 6 Sound velocity contour plots of different polymers with a –C–C– backbone. All samples are stretched to a draw ratio of ≈ 7. Polyethylene reaches the highest modulus, while polypropylene (- - -) has a slightly lower value for C_{33} P4M1P (— · — · —) shows almost isotropic behaviour when compared to the other materials.

polarized electric field. The elastic deformation averages force constants on a molecular level [26, 27]. In the case of P4M1P, the perpendicular contribution is also large. The WAXS diffraction patterns measured for some of our samples ($\lambda \approx 5$, Fig. 7) are similar to the photographs presented by He and Porter [25] for draw ratios between 11 and 20. This concludes that in

TABLE II Resulting elastic constants for oriented P4M1P. The transverse mode was not observed at $\lambda = 1$. Because of the cylindrical shape of the ultra-highly oriented sample, only the data parallel and perpendicular to the stress direction have been evaluated

λ	C_{11}	C_{13}	C_{33}	C_{44}
1.00	4.090	–	–	–
4.29	3.415	2.149	5.297	1.090
5.37	3.294	2.066	5.197	0.993
5.86	3.340	2.093	5.279	1.003
6.52	3.368	2.085	5.320	0.973
≃ 60	3.299	–	5.626	–

the case of P4M1P extrusion and uniaxial deformation by drawing are not comparable, in contrast to PP [6]. The effective draw ratio of the P4M1P rod sample compared to uniaxial stretching could be estimated to be approximately 20.

Sakurada and Kaji estimated a maximum chain elastic modulus from the (0 0 1) crystal plane of 6.7 GPa [28]. The observed macroscopic modulus was approximately one-third of this maximal value [25]. The modulus determined from the velocities of hypersound at approximately 10 GHz ($C_{33} \approx 5.3$GPa) is about 80% of the crystal modulus, i.e. still lower. This is due to the contribution of the glassy amorphous phase. With lower elastic constants compared to the average elastic constants of PE and PP ($C_{11} \approx 5.7$ GPa) at hypersound frequencies, P4M1P remains nearly isotropic (Fig. 5b). The helical conformation of the molecules (7*2/2 [25]) together with the bulky side groups provide a predominantly isotropic distribution of covalent bonds.

The relative scattered intensities measured for P4M1P are shown in Fig. 8. Because the relative intensities of the transverse lines are much smaller in P4M1P compared to PP, the relative error of the measurement is larger for this material. Nevertheless, as the fitting procedure converged to reasonable and unique values for all degrees of deformation, the changes of the photoelastic constants are significant. We estimate that the experimental error is about one order of magnitude larger than the error of the position of the lines, which is about 0.5%.

The dependence of photoelastic constants of PP and P4M1P on deformation is plotted in Fig. 9. Both materials show a characteristic behaviour of the photoelastic constants. For equal indices, they seem to display a parabolic dependence while for different indices the variation is more linear.

Nelson and Lax have formulated the theory of the photoelastic interaction for non-ferroelectric anisotropic materials [29]. They divided this effect into symmetric, antisymmetric, indirect and direct parts. The indirect as well as the antisymmetric contribution must not be considered in the case of P4M1P, because in the hexagonal systems of the 6/mmm class (Hermann and Maugin) no piezo-electric and electro-optic contributions exist. Furthermore, Ullrich [30] has found that the electro-optic Kerr effect in oligomers of the olefins is many orders of magnitude lower than in

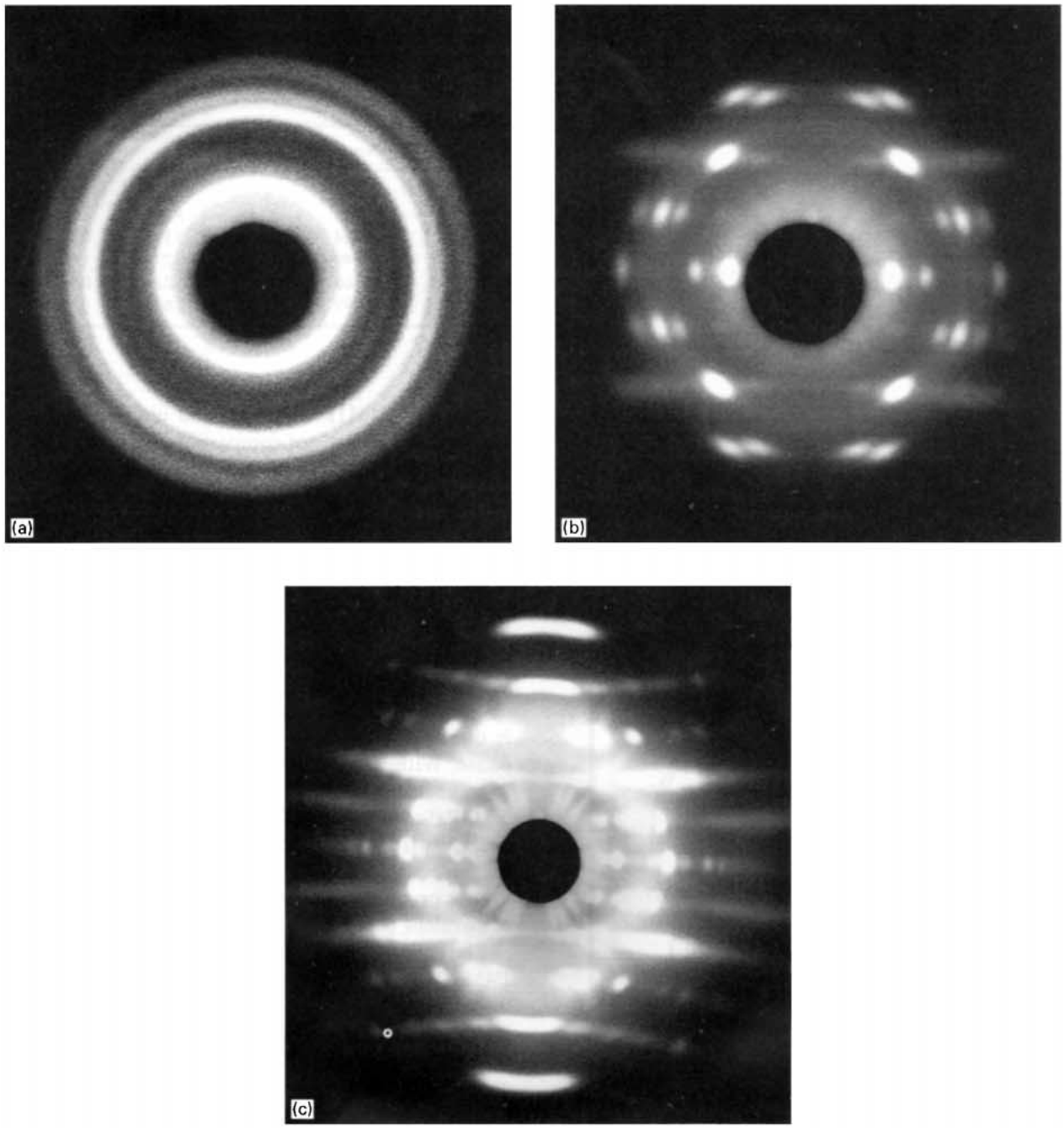

Figure 7 WAXS diffraction pattern of the P4M1P samples: (a) the undrawn film, (b) the oriented film ($\lambda = 5.8$), and (c) the extruded rod.

polar crystals and therefore will not contribute to Brillouin scattering. We will discuss, below, the direct and symmetric contribution to the photoelastic effect. The piezo-electric and electro-optic contribution of this part is also zero, similar to the indirect contribution above.

There are three contributions to the direct and symmetric photoelastic constants. The first one is identical for all tensor components. It is related to the density of the material, as it represents the change in the number of oscillators per unit volume. This contribution can be neglected in the case of P4M1P because the density did not change.

The second one holds for the diagonal elements of the photoelastic tensor. It can be interpreted in two different manners as it is related to the resonance frequency of the polarizability into a particular direction. In the case of PP, the probing of the polarizability at different draw ratios is done at different frequencies by the change of C_{33}. Therefore, the change of p_{33} can be interpreted as a modulation of the resonant strength of the interaction caused by a change of the excitation frequency, but a change of the resonant frequency due to the deformation cannot be ruled out. The change in p_{11} is therefore due to the change of the resonant frequency, because C_{11} is almost unchanged by drawing. This also holds for p_{11} and p_{33} in P4M1P.

The last one affects the non-diagonal components, p_{ij}, of the photoelastic tensor. It comes from the coupling of the oscillation in direction i with the oscillation in direction j due to the deformation caused by the sound wave.

The deformation of a sample by uniaxial streching will not only cause orientation of the crystalline parts,

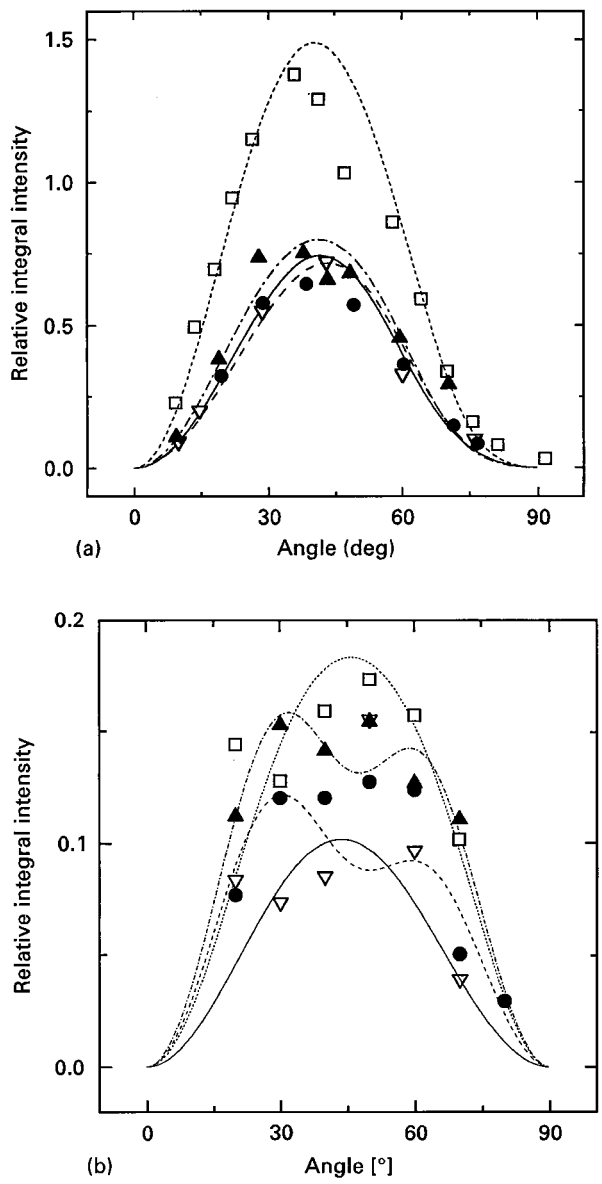

Figure 8 Relative integral scattered intensities of the Brillouin lines in polypropylene and P4M1P. Note that the relative intensities P4M1P are almost one order of magnitude smaller compared to PP. The values for P4M1P are, though small, significant and evaluable. λ: (a) 3.4, (- - ● - -) 4.9, (— · — ▲ — · —) 5.8, (- - □ - -) 7.3, (b) (—▽—) 4.3, (- - ● - -) 5.4, (— · — ▲ — · —) 5.9, (— — □ — —) 6.5.

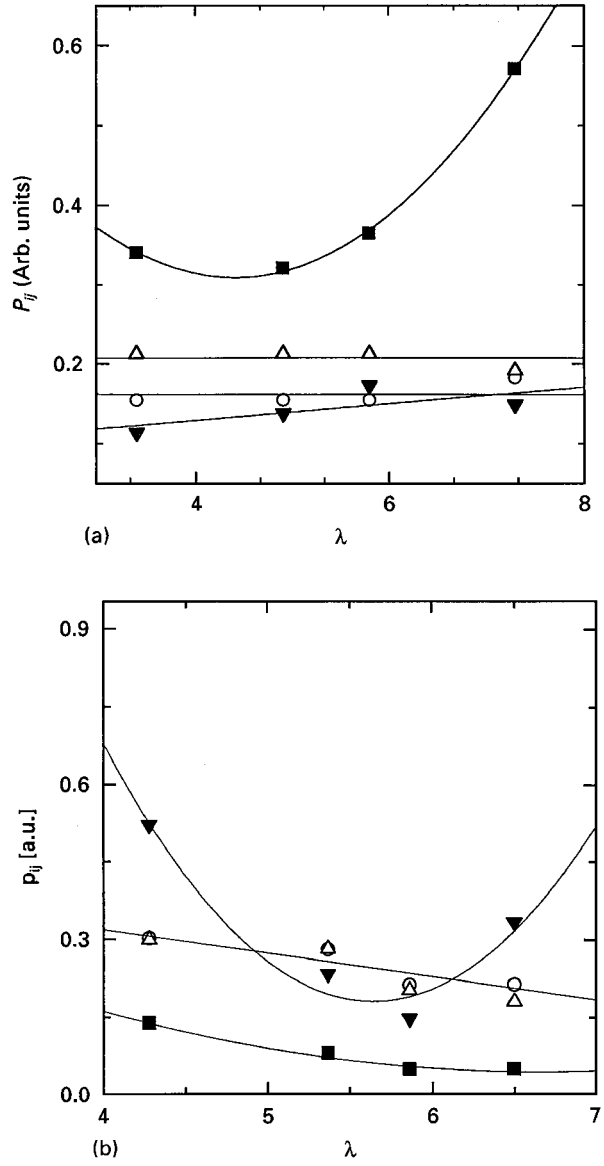

Figure 9 Photoelastic constants of (a) PP and (b) P4M1P. (■) p_{11}, (○) p_{13}, (△) p_{31}, (▼) p_{33}.

TABLE III Photoelastic constants for oriented P4M1P. The transverse mode was not observed at λ = 1

λ	p_{11}	p_{13}	p_{31}	p_{33}
4.29	0.138	0.302	0.300	0.521
5.37	0.080	0.281	0.282	0.233
5.86	0.049	0.212	0.202	0.146
6.52	0.064	0.213	0.180	0.333

but also a deformation of them due to stress. This deformation is added to the deformation due to the sound wave, changing the resonant frequency of the interaction or its strength.

4.1. Photoelastic constants of PP

In this material, extrusion and uniaxial drawing are equivalent [6]. As the changes of p_{13} and p_{31} are small they were regarded as constant by Wang and co-workers. Because, in the extruded samples, these components are changing, we re-evaluated the data from their work using the values measured with the extruded samples for better accuracy. p_{13} and p_{31} remain constant for most draw ratios, only for large deformations do they change in the opposite direction, while the sum of both is unchanged. As they reflect the change of the coupling of the polarizability oscillations parallel and perpendicular to the stress, this can be explained by a directional sorting of orientational invariant units. Surprisingly, during deformation, p_{33} stays apparently unchanged, although C_{33} is enlarged by almost one order of magnitude above the isotropic value during stretching. On the other hand, p_{11} displays significant variation, although C_{11} is almost constant during deformation. Therefore, in the stress direction (along the chains) the phonon frequencies are far away from the resonance frequencies responsible for the scattering, while in the perpendicular direction the resonant frequency is very dependent upon deformation, although the probing phonon frequency is nearly constant.

4.2. Photoelastic constants of P4M1P

This material shows a completely different behaviour in comparison with PP, even though its monomer is also of the vinyl type. p_{13} and p_{31} (Table III) decrease simultaneaously, which is not an effect of decreasing laser intensity as the Rayleigh intensity remains constant (cf. Fig. 3a and b). This could be due to structural changes. A sorting of the polarizibilities (i.e. orientational invariant units) is not probable. This corresponds to the constancy of birefringence. The behaviour of p_{11} and p_{33} is reverse compared to PP. p_{11} remains virtually unchanged, while p_{33} displays a strong correlation with λ. This behaviour is easier to understand, because most changes during stretching are expected to be parallel and not perpendicular to the drawing direction. This indicates that the chains in this case are deformed, and that the resonance frequency of the interaction between light and sound is changed due to this deformation. Perpendicular to the drawing direction this effect is small and comparable to the change of C_{11}. Deutsch and Heise have observed one new X-ray reflex [31] which is observable only in the deformed state. It is near the primary beam and therefore corresponds to a superstructure formed through the deformation process, namely the formation of the neck. Because the internal draw ratio in the necked region is much larger than outside, the chains are most probably fully oriented when passing the necked region. This indicates that further deformation will not take place by the orientation of crystalline aggregates, but by a combination of deformation and slipping of the chains. On slipping, the overall mechanical properties of the material perpendicular to the draw direction will not change much, because they are ruled by the side groups, as well as the resonant frequency of the photoelastic interaction. In contrast the coupling of the vibrations parallel and perpendicular to the drawing direction will decrease on slipping, which explains the behaviour observed with p_{13} and p_{31}. The correlation of p_{33} with the draw ratio is therefore due to deformation of the chains.

5. Conclusions

Brillouin scattering is a tool for measuring the elastic constants of a sample. Additionally, it allows changes of the photoelastic tensor to be monitored. For special sample and scattering geometries [6, 21] even absolute measurements of this material property are possible. Its change on deformation is very distinct, even between similar materials like PP and P4M1P. The theory required to understand these changes is more detailed compared to continuum mechanics used to evaluate the elastic constants. The task is reduced significantly for the considered polymers, as the density remains constant and electro-optic effects can be ruled out. The photoelastic effect, as well as the sound velocity anisotropy and birefringence, seem to be dominated by the side groups of the polymers. In the case of P4M1P both the mechanical and optical anisotropy are nearly balanced between side groups and the main-chain contribution. The use of side-groups effects, in order to control average material properties, seems promising.

Acknowledgements

We thank Mitsui for providing the film sample, Professor Kamamoto for providing the P4M1P-rod, M. Asbach and M.-L. Kienzle for performing the density measurements, K. Hoffmann for making the WAXS images and K. Hartmann for the assistance with the tensile apparatus. This work was supported by the Deutsche Forschungsgemeinschaft (Sonderforschungsbereich 239, Projekt B9).

References

1. L. PEETZ, J. K. KRÜGER and M. PIETRALLA, *Coll. Polym. Sci.* **256** (1987) 761.
2. Q.-L. LIU and C. H. WANG, *Macromolecules* **16** (1983) 482.
3. R. WEEGER, M. PIETRALLA, L. PEETZ and J. K. KRÜGER, *Coll. Polym. Sci.* **266** (1988) 700.
4. L. PEETZ, Dissertation, Saarbrücken (1987).
5. C. H. WANG, Q.-L. LIU and B. Y. LI, *J. Polym. Sci. B Polym. Phys.* **25** (1987) 485.
6. D. B. CAVANAUGH and C. H. WANG, *J. Appl. Phys.* **53** (1982) 2793.
7. R. J. ADAMIC and C. H. WANG, *Macromolecules* **17** (1984) 2018.
8. H. H. KRBECEK, "Untersuchung der elastischen Eigenschaften anisotroper Polymere im Hyperschallbereich mit Hilfe hochauflösender Brillouin spektroskopie" (Shaker, Aachen, 1994).
9. H. H. KRBECEK, W. KUPISCH and M. PIETRALLA, *Polymer* **37** (1996) 3483.
10. J.-P. JARRY and G. D. PATTERSON, *J. Polym. Sci. B Polym. Phys.* **19** (1981) 1791.
11. C. H. WANG G. FYTAS and J. ZHAN, *J. Chem. Phys.* **82** (1985) 3405.
12. A. ONABAJO and T. DORFMÜLLER, *J. Polym. Sci. B Polym. Phys.* **25** (1987) 749.
13. G. FYTAS, Y. H. LIN and B. CHU, *J. Chem. Phys.* **74** (1981) 3131.
14. Y. ITAGAKI, O. OHTSU, K. TAMAKA, M. TAKEDA and T. KANAMOTO, *Rep. Progr. Polym. Phys. Jpn* **30** (1987) 329.
15. T. KANAMOTO and O. OHTSU, *Polym. J.* **20** (1988) 179.
16. "TPX Polymethylpentene Technical Information No. 1" (Mitsui Petrochemical Industries, 1985).
17. J. K. KRÜGER, in "Optical Techniques to characterize Polymer Systems", p. 429, H. Bässler (Ed.) (Elsevier, Amsterdam, 1989).
18. K. PEARSON, *Philos. Trans.* **216A** (1916) 429.
19. W. H. PRESS, "Numerical Recipes in Pascal" (Cambridge University Press, Cambridge, 1989).
20. B. A. AULD, "Acoustic fields and waves in solids" (Wiley, New York, 1973).
21. R. VACHER and L. BOYER, *Phys. Rev. B* **6** (1972) 639.
22. B. J. BERNE and R. PECORA, "Dynamic Light Scattering" (Wiley, New York, 1976).
23. F. POCKELS, *Göttinger Abh.* **39** (1893).
24. J. F. NYE, "Physical Properties of Crystals" (Oxford University Press, Oxford, 1969).
25. T. HE and R. S. PORTER, *Polymer* **28** (1987) 946.
26. S. H. ANDERS, H. H. KRBECEK and M. PIETRALLA, *J. Polym. Sci. B. Polym. Phys.* **35** (1997) 1661.
27. R. J. LEYRER and G. WEGNER, *Ber. Bunsenges. Phys. Chem.* **82** (1978) 697.
28. I. SAKURADA and K. KAJI, *J. Polym. Sci. C* **31** (1970) 57.
29. D. F. NELSON and M. IAX, *Phys. Rev. B* **3** (1971) 2778.
30. K. ULLRICH, Dissertation, Darmstadt (1984).
31. B. DEUTSCH and B. HEISE, to be published.

Received 15 January 1997
and accepted 2 April 1998